Polymer 126 (2017) 368–375

Contents lists available at ScienceDirect

Polymer

journal homepage: www.elsevier.com/locate/polymer

Effect of humidity on surface structure and permeation of triblock terpolymer derived SNIPS membranes

Yuk Mun Li [a, b, 1], Qi Zhang [a, 1], Juan R. Álvarez-Palacio [a], Ilhem F. Hakem [c], Yibei Gu [a], Michael R. Bockstaller [c], Ulrich Wiesner [a, *]

[a] Department of Materials Science and Engineering, Cornell University, Ithaca, NY 14850, United States
[b] Robert Frederick Smith School of Chemical and Biomolecular Engineering, Cornell University, Ithaca, NY 14850, United States
[c] Department of Materials Science and Engineering, Carnegie Mellon University, 5000 Forbes Ave., Pittsburgh, PA 15213, United States

ARTICLE INFO

Article history:
Received 11 February 2017
Received in revised form
12 May 2017
Accepted 15 May 2017
Available online 17 May 2017

Keywords:
Self-assembly
Triblock terpolymer
Membranes

ABSTRACT

Block copolymer (BCP) ultrafiltration (UF) membranes derived from a hybrid process of BCP self-assembly and non-solvent induced phase separation (SNIPS) exhibit an asymmetric structure consisting of ordered pores in a selective skin layer above a highly permeable substructure. In this work, we investigate relative humidity (RH) as a casting condition that influences poly(isoprene-*b*-styrene-*b*-4-vinylpyridine) (ISV) membrane surface structure in terms of order and uniformity. An optimum RH of 40–45% is determined to produce membranes characterized by a high density of square packed pores with a narrow pore size distribution. Membranes cast at lower and higher RH show a drop off in order and uniformity. The RH dependent structural changes correlate well with small molar mass dye solute (methyl orange; molar mass of 327 g/mol) diffusion rates. Membranes cast at 40% RH reveal higher diffusivity than when cast at 75% RH. The rate of permeation is further controlled via pH dependent pore closure as well as through ISV terpolymer molecular architecture with increasing solute diffusivity observed in membranes cast from increasing terpolymer molar mass. Experimental findings on small molar mass solute permeability can only be accounted for when compared with theoretical predictions from a hydrodynamic theory combined with the effects of tortuosity when a simplified membrane structure is assumed. Results suggest that SNIPS derived BCP membranes may have potential for applications in drug delivery.

1. Introduction

Polymeric membranes fabricated via block copolymer (BCP) self-assembly plus non-solvent induced phase separation (SNIPS) [1] process rise as strong candidates for next generation asymmetric ultrafiltration (UF) membranes due to their advantageous combination of uniform pore size and high pore density. The highly ordered mesoporous surface with narrow pore size distribution promises high resolution while the high pore density together with the macroporous substructure gives rise to high permeability. Since the first publication on SNIPS membranes derived from BCP poly(styrene-*b*-4-vinylpyridine) (SV) in 2007 [2], the SNIPS process has been studied extensively for various BCPs over the past decade.

A primary focus in the emerging SNIPS derived BCP membrane field to date has been the exploration of membrane properties through molecular design. Functionalizing membranes through molecular architecture rather than process control is a paradigm shift in the membrane field and promises substantial expansion of membrane capabilities. For example, BCP membranes containing a poly(4-vinylpyridine) (P4VP) or poly(acrylic acid) (PAA) block are pH-responsive [2–4] resulting in changes in effective pore size upon pH variations. Mechanical properties like membrane toughness can be largely enhanced through the addition of a rubbery polyisoprene block to the high glass transition (T_g) matrix block of BCP UF membranes [3]. For foreign molecule attachment, membranes can be designed with covalent binding sites by e.g. adding a functional group at the hydrophilic chain end decorating the pore walls allowing for thiol-ene click chemistry based post-fabrication steps [5]. Lastly, the blending of two (or more) BCPs into the casting dope enables a novel “mixing and matching” approach for e.g.

* Corresponding author.
E-mail address: ubw1@cornell.edu (U. Wiesner).
[1] These authors contributed equally to this work.

http://dx.doi.org/10.1016/j.polymer.2017.05.037
0032-3861/

tailoring of membrane surface chemistry from different polymers [6].

Another main focus of SNIPS membrane studies has been the structure control of the selective top separation layer. Although first systematic studies regarding control of SNIPS membrane substructure are emerging [7], the overwhelming majority of reports has the regularly patterned, self-assembled mesopores at the top surface at the center of attention. For a number of BCP systems casting conditions have been tested to achieve a regularly patterned surface structure including casting dope composition, evaporation time, and coagulation bath conditions [8–10]. Other studies have focused on the tuning of pore size by varying BCP molar mass or through the incorporation of additives [9,11]. Finally, several studies elucidate the formation mechanisms of these well-organized selective layers [3,12–15]. Most recently, *in-situ* grazing incidence small angle x-ray scattering (GISAXS) has been employed to better understand the structure evolution during organic solvent evaporation steps [16–18], revealing structural phase transitions in the top separation layer [17].

Despite numerous studies of parameters affecting SNIPS membrane structure and membrane formation mechanisms, systematic investigations of the relationship between surface structure and membrane performance as well as comparisons and benchmarking with existing UF membranes in terms of achievable resolution are still limited. In previous work, polyethylene oxide (PEO) or protein rejection and flux tests have been used to characterize membrane performance. Rejection tests have mainly been employed for pore size characterization via molecular weight cut off (MWCO) curves [3] while permeability has been assessed via flux tests. To move the use of SNIPS membranes beyond conventional separation applications and towards protein or drug delivery vehicles, and inspired by studies of single file diffusion through nanochannels for protein delivery applications [19], it is interesting to characterize the diffusion of small molar mass solutes through asymmetric SNIPS membranes as a function of membrane structure. To that end, in the present study we first investigated the effects of relative humidity (RH) on surface structure of SNIPS derived UF membranes from poly(isoprene-*b*-styrene-*b*-4-vinylpyridine) (PI-*b*-PS-*b*-P4VP, ISV) and subsequently correlated the observed structural changes with the permeation of a model dye solute through the BCP membranes thereby identifying parameters that tailor the rate of diffusion.

To the best of our knowledge, this is the first report on the influence of RH on the top surface structure of SNIPS derived UF membranes. Results demonstrate that ISV based membrane top surface structure is sensitive to RH and reaches an optimum at mid-range RH around 40–45%, while higher or lower humidity disturbs the surface structure. Interestingly, it is observed that higher casting solution concentrations render the membranes less sensitive to RH changes. Top surface structural changes directly correlate with model small molar mass dye solute permeation rates, with membranes cast at optimum mid-range RH possessing higher diffusivities. Additional control over the rate of small model solute diffusion is achieved through parent terpolymer molar mass as evidenced by membranes fabricated under RH conditions providing optimized surface structures. Finally, measured membrane permeability is compared to theoretical predictions to account for the experimental observations.

2. Experimental

2.1. Polymer synthesis

Three ISV triblock terpolymers were synthesized via sequential anionic polymerization as previously described [8]. The polymers were characterized by gel permeation chromatography (GPC) and ^{1}H NMR for molar mass (M_n), volume fractions of each block (f), and polydispersity index (PDI). A summary of characterization results for each ISV triblock terpolymer used in this study is provided in Table 1.

2.2. Membrane fabrication

ISV terpolymers were dissolved in a binary solvent system of 1,4-dioxane (DOX) and tetrahydrofuran (THF) in a 7/3 wt ratio and appropriate concentrations (see results and discussion section). The SNIPS process was conducted inside a drybox following these steps: 1) the casting solution was pipetted onto a substrate (glass or nylon support); 2) a thin film was cast with a doctor blade at a gate height of 220 μm; 3) solvent evaporated for a specified amount of time, and 4) the film was immersed into a water coagulation bath. Levels of RH inside the drybox were controlled by either introducing a hot water bath or sparging with dry N_2 to increase or decrease RH, respectively. A humidity meter (Model: VWR-61161-378) was used to monitor RH during casting. Levels of RH were adjusted before casting. The stream of dry N_2 was stopped before the start of the casting process to prevent air disturbances during the evaporation step. Humidity fluctuations during the evaporation step were within ± 2% RH.

2.3. Scanning electron microscopy (SEM)

Scanning electron microscopy (SEM) images of membranes were acquired on a Tescan LM Mira3 FE-SEM with an in-lens detector. Pore size distributions and Fast Fourier transform (FFT) analyses of the top surfaces were performed via ImageJ with the Radial Profile Extended plugin (Philippe Carl). For comparison, the pore size data was fitted with both a normal Gaussian distribution and a log-normal distribution using Matlab's fitting tool with the bin width set to 1.

2.4. Membrane permeation studies

The permeation of a model dye solute, methyl orange, through the series of ISV based triblock terpolymer membranes was evaluated in a side-by-side diffusion cell (PermeGear). The setup (Fig. 1) consisted of two chambers, the donor (right chamber) and receptor (left chamber) cell, with a volume of 3 mL each and containing a magnetic stirrer. The terpolymer membrane was placed between the two chambers with the selective surface layer facing the donor cell. The setup was sealed by clamping the cells tightly together and placed on a stir plate with a continuous stir rate of 200 rpm. The donor cell was filled with 3 mL of a methyl orange solution (1.0 mg methyl orange per mL buffer solution of the respective pH) while the receptor cell was filled with the same volume of the respective buffer solution. For membrane "closed state" studies, pH = 4 buffer solutions were prepared with sodium acetate and acetic acid. For membrane "open state" studies, pH = 7 buffer solutions were prepared with imidazole and hydrochloric acid. 0.1 M buffer solutions were tested with a pH probe before conducting experiments. Receptor cell aliquots (300 μL) were taken every 20 min for three

Table 1
Summary of ISV terpolymer characteristics.

Polymer	M_n (kg/mol)	f_{PI}	f_{PS}	f_{P4VP}	PDI
ISV43	43	0.24	0.56	0.20	1.02
ISV99	99	0.23	0.63	0.14	1.20
ISV119	119	0.19	0.65	0.16	1.17

*Number average molar mass (M_n), volume fraction (f), and polydispersity index (PDI).

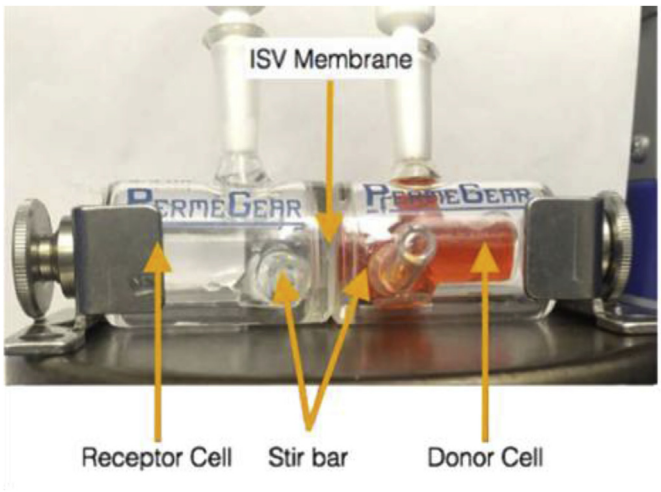

Fig. 1. Experimental setup for membrane permeation studies: side-by-side stirred cell.

hours for "open state" experiments and every 20 min for four hours for "closed state" experiments. Receptor cell aliquots were replaced with the same volume of the corresponding buffer solution.

The concentration of diffusant (methyl orange) was measured using a UV-VIS spectrophotometer (Varian Cary Model 5000) at a wavelength of 480 nm. Concentrations were determined based on standard curves of methyl orange. The diffusion constant of methyl orange can be determined from the cumulative mass $Q(t)$ of permeant passing through the membrane. The relevant relation is obtained by integration of the flux through the membrane (which is given by the well-known solution to Fick's second law for solute diffusion through pores) and reads as [20]:

$$Q(t) = C(\varepsilon A)(\tau l)\left\{\frac{Dt}{(\tau l)^2} - \frac{1}{6} - \frac{2}{\pi^2}\sum_{n=1}^{\infty}\frac{(-1)^n}{n^2}e^{-n^2\pi^2\frac{Dt}{(\tau l)^2}}\right\} \quad (1)$$

Here, $Q(t)$ describes the cumulative mass of solute at time t. (εA) is the effective pore area of the membrane (ε is the porosity of the membrane and $A = 1.54\ \mathrm{cm}^2$). (τl) is the length of the tortuous path (with τ being the tortuosity). C is the concentration of solute (methyl orange) in the donor cell ($C = 1$ mg/mL) and D is the diffusion coefficient (in our results section also referred to as D(exp)). In the limit of large time t (*i.e.* in the case of the steady state), $Q(t)$ simplifies to:

$$Q(t) = C(\varepsilon A)\frac{D}{\tau l}\left\{t - \frac{(\tau l)^2}{6D}\right\} \quad (2)$$

Equation (2) has an intercept on the *t-axis*, referred to as the "time lag" [21], or t_{lag}, that follows as,

$$t_{lag} = \frac{(\tau l)^2}{6D} \quad (3)$$

The steady state permeability, P (also referred to as P(exp) in our results section), for the transport of the permeant through the pores of the membrane can be evaluated by dividing Eqn. (2) by the concentration C and evaluating the time derivative to get:

$$P = \frac{1}{AC}\frac{dQ(t)}{dt} \equiv \frac{\varepsilon D}{\tau l} \quad (4)$$

Note that either Eqn. (3) or Eqn. (4) can be applied to get the diffusion constant of solutes from the cumulative mass measurements (i.e. $D(\mathrm{exp}) = P\tau\ l/\varepsilon$). If a lag time can be obtained experimentally (*i.e.*, if t_{lag} is in the range of conveniently accessible timescales), then analysis of Eqn. (3) is generally the preferable approach since only knowledge of the tortuosity is required.

Since in the presence of nano-sized pores, hydrodynamic effects on the mobility of the solute molecules cannot be excluded. Therefore, the theoretical effective diffusion coefficient of methyl orange diffusing in the membranes, $D(\lambda)$, was determined using Renkin's hydrodynamic model (which describes the diffusion of a solid, spherical solute through an array of cylindrical pores with comparable size) valid for $0 \leq \lambda < 0.4$ [22]:

$$D(\lambda) = (1-\lambda)^2\left(1 - 2.104\lambda + 2.09\lambda^3 - 0.95\lambda^5\right)D_w \quad (5)$$

where λ is the solute-to-pore ratio (r_s/r_p) and D_w is the diffusivity of methyl orange dye in water. The first term in Eqn. (5), known as the 'steric factor', describes the restriction of the solute molecules entering into the pores (given by the ratio of the effective area $\pi(r_p - r_s)^2$ to the actual area πr_p^2). The second term describes the effect of the viscous drag due to the wall once the diffusant enters the pore. Membrane pore size was determined through image analysis of SEM micrographs using the ImageJ package. The solute size (in nm) was calculated by Ref. [23]:

$$log_{10}(r_s) = -1.3363 + 0.395log_{10}(M_w) \quad (6)$$

where M_w is the molar mass of methyl orange (327 g/mol).

Eqn. (6) yields a solute radius equal to 0.45 nm, in good agreement with the value, $r_s = 0.47$ nm, obtained from a geometrical approximation ($r_s = (3M_w/(4\pi\rho N_{Av}))^{1/3}$), where $\rho = 1.28$ g/mL denotes the density of methyl orange at $T = 25\ ^\circ$C and N_{Av} is the Avogadro number [22], and an experimental value of $r_s = 0.40$ nm in NaCl solution [24].

The permeability coefficient, $P(\lambda)$, can be estimated theoretically as follows:

$$P(\lambda) = \frac{\varepsilon D(\lambda)}{\tau l} \quad (7)$$

3. Results and discussion

3.1. Effect of relative humidity (RH) on membrane top surface structure

The quality of the top surface pore structure is a key factor with regards to the high-performance of SNIPS derived UF membranes. SNIPS membranes are of particular interest due to their highly ordered mesopores derived from BCP self-assembly leading to high pore densities and uniform pore size. The casting conditions to achieve membranes with an optimum surface structure, including solvent system, solution concentration, evaporation time, etc., have been studied extensively. In this work, we evaluated another crucial, yet easy-to-ignore factor – relative humidity (RH).

ISV SNIPS membranes were cast inside a drybox as detailed in the experimental section. Inside the drybox, RH was controlled during the casting process by introducing water vapor or sparging with dry N_2. A humidity meter was used to determine RH during the evaporation process.

A membrane series from a solution of 9 wt% ISV119 in a 7/3 DOX/THF solvent mixture was produced by casting membranes at different RH employing an evaporation time of 200 s. Resultant membrane top surface structures as revealed by scanning electron microscopy (SEM) are shown in the top row of Fig. 2. Associated FFT analyses of these SEM images are shown in Fig. 3a.

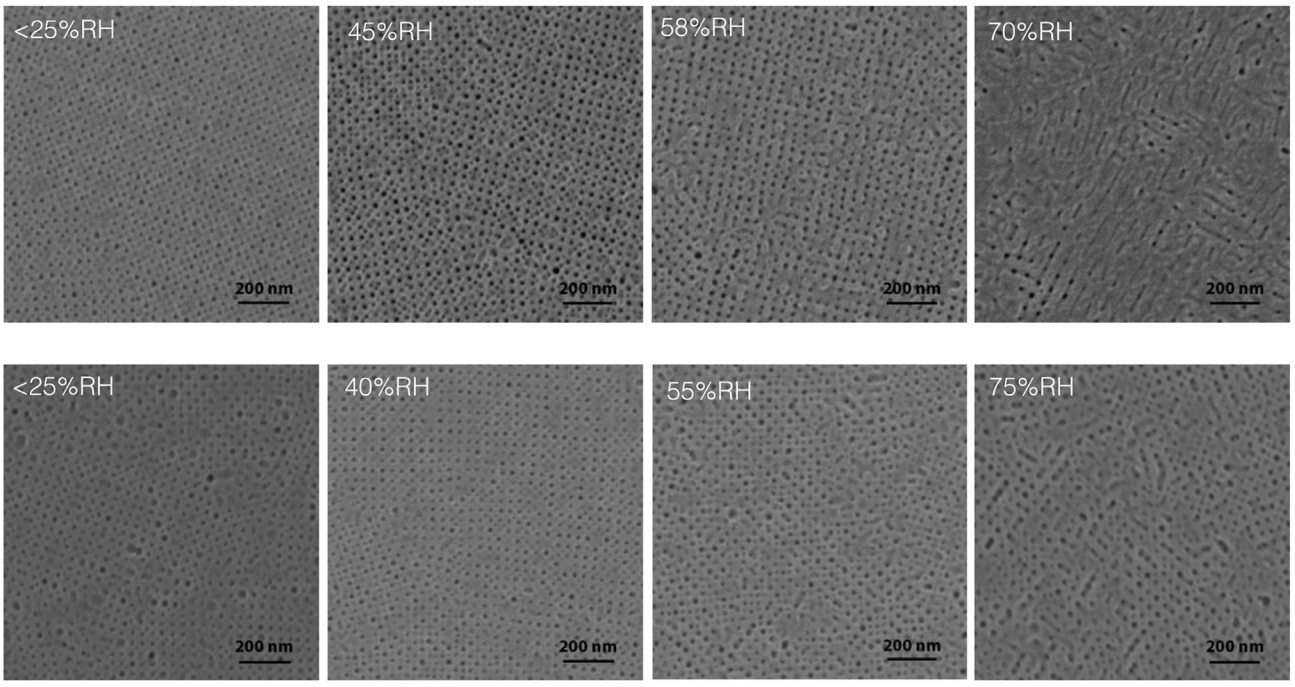

Fig. 2. SEM micrographs of ISV119 membrane top surfaces cast at varying RH Membranes in the top row were obtained from a solution of 9 wt% ISV119 in a 7/3 DOX/THF solvent mixture and an evaporation time of 200 s. Membranes in the bottom row were fabricated from a solution of 11 wt% ISV119 in 7/3 DOX/THF solvent system cast onto 0.1 μm nylon supports with an evaporation time of 100 s.

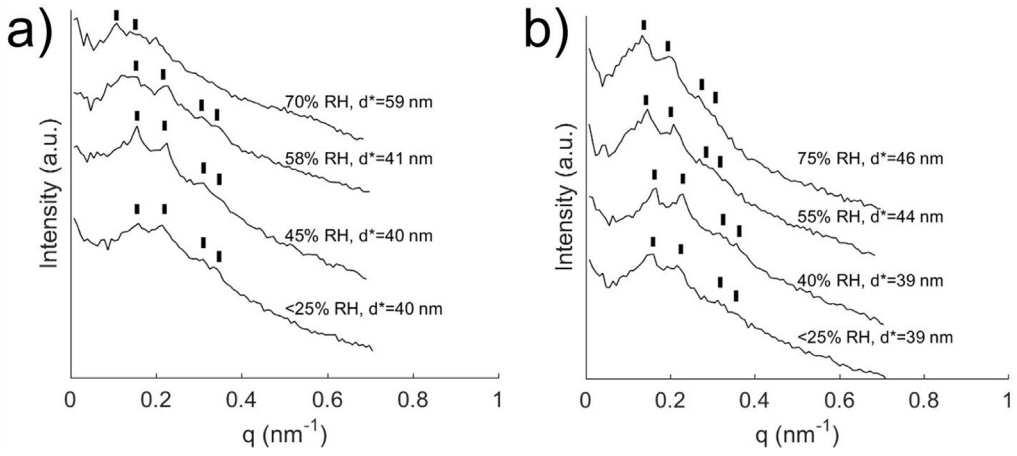

Fig. 3. Radially integrated FFTs of SEM images of ISV119 membranes cast at varying RH from polymer casting solutions of a) 9 wt% and b) 11 wt%.

From the SEM images, top surfaces exhibited open and highly ordered pores with few defects when cast at 45% RH. FFT analysis confirmed pores packed in a 2D square lattice consistent with previous reports on ISV membranes [3,25]. At low humidity, (<25% RH), the top surface retained a well-ordered structure but with less open pores as compared to membranes cast at 45% RH. Increasing the humidity to 58% resulted in the presence of wormlike defects in the top surface. By further increasing the RH to 70%, top surface structure deteriorated substantially and assignment of a pore lattice from the associated FFT analysis is difficult. This series of membrane top surface structures suggested that the optimum RH value for casting ISV SNIPS membranes is at ~45%, with deterioration of the ordered pore surface structure when moving in particular to higher RH.

A second RH series was performed from a more concentrated ISV polymer solution. A solution of 11 wt% ISV119 in 7/3 DOX/THF solvent system was cast onto 0.1 μm nylon supports with an evaporation time of 100 s. The corresponding membrane top surface SEM images are shown in the bottom row of Fig. 2. From these SEM images, the optimum RH remained to be around 40%, while this time higher and lower RH lead to an increase in surface defects. Furthermore, when compared with results of the 9 wt% ISV series, the 11 wt% ISV image series does not present as much of a surface structure disruption as RH is increased to 70% or above. This is also reflected in the FFT analyses (Fig. 3), exhibiting improved lattice formation for higher RH values when moving from 9 wt% to 11 wt% ISV solutions. At RH above 70%, it was not possible from the FFT analysis to assign a lattice of the membrane cast from 9 wt%

solution, while the counterpart from 11 wt% solution matched well with a square lattice. SEM top surface images were further analyzed for pore size distribution using ImageJ as shown in Fig. 4. Results reveal that the membrane cast at 40% RH has the smallest average pore size when compared to membranes cast at <25%, 55%, and 75% RH. Furthermore, the membrane cast at 40% RH also exhibits a substantially narrower pore size distribution which is crucial for achieving high-resolution in separation processes. The coefficient of variation, σ/μ (ratio of standard deviation, σ, and mean, μ), is smallest in membranes cast at 40% RH ($\sigma/\mu = 0.36$, 0.28, 0.36, and 0.38 for 25%, 40%, 55%, and 75% RH, respectively, for normal Gaussian fits and $\sigma/\mu = 0.14$, 0.12, 0.14, and 0.15 for 25%, 40%, 55%, and 75% RH, respectively, for log-normal distributions [26]).

The FFT analyses of the top surface SEM images also allowed us to quantify the respective pore-to-pore distances, d^*. Comparing results in Fig. 3a and b for both 9 wt% and 11 wt% ISV humidity series suggests that with increasing humidity, d^* increases. While values for d^* stay unchanged for low (<25%) and mid range (45% and 40%) RH, increasing RH further to first 58% or 55%, and then to 70% or 75%, increases d^* substantially. This increase in pore-to-pore distance results in a concomitant decrease in surface pore density, see results for the 11 wt% ISV series in Table 2. Therefore, when assuming a constant pore size and pore size distribution, membranes cast at RH around 45% not only have more well defined top surface layers with narrower pore-size distributions expected to provide higher resolution, they should also be more permeable as a result of higher pore densities.

Table 2
Pore density of humidity series cast from 11 wt% solution.

Humidity	Pore density (x10^{14} pores/m^2)
<25%RH	6.8
40%RH	8.0
55%RH	6.7
75%RH	5.1

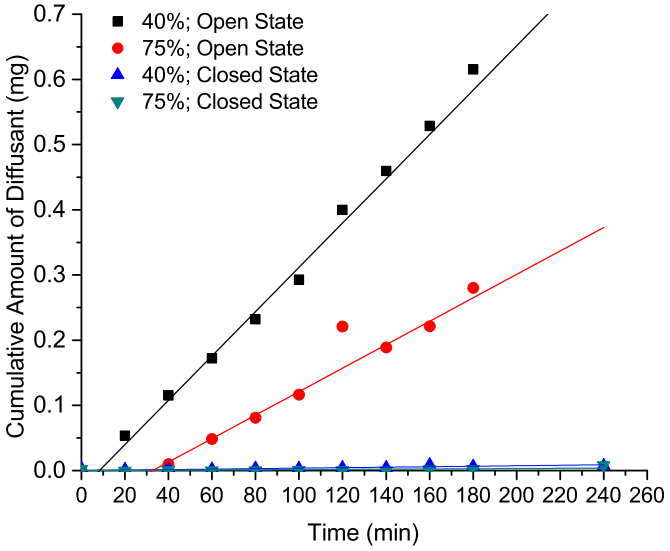

Fig. 5. Cumulative amounts of methyl orange permeated through ISV119 membranes cast at 40% and 75% RH in open and closed states. Lag-times for ISV119 membranes in the open state are 8.3 min and 33 min for membranes cast at 40% and 75% RH, respectively (Table 3).

3.2. Permeation studies of small molar mass model solute

3.2.1. Influence of relative humidity on permeation

We investigated the effect of RH on solute transport properties of ISV119 membranes (11 wt%; 100s evaporation time) cast at 40% and 75% RH conditions. Fig. 5 shows the cumulative amounts of methyl orange dye permeated through ISV119 membranes at neutral pH, i.e. at a pH where the poly(4-vinlypyridine) chains are unprotonated and the pores therefore open, as compared to pH = 4, i.e. a pH at which protonation leads to chain stretching and therefore to closed pores (pK_a(P4VP) = 4.6) [3]. The values of the diffusion coefficient, D(exp), calculated from the time-lag method (Eqn. (3)), for the open states are listed in Table 3. A convexity or lag-time can be observed at short elapsed times before the system reaches a pseudo-steady state. The permeation rate of methyl orange is higher by almost a factor 4 in membranes cast at the optimized RH of 40% as compared to membranes cast at 75% RH. The higher permeation rate is consistent with the more highly ordered surface structure with fewer defects and resulting higher pore density of more narrowly size-distributed pores. On the time scale of the experiments, membranes in the closed state at pH = 4 were not permeable at all to the small molar mass solute methyl orange.

3.2.2. Influence of pore size on permeation

To gain a greater understanding of the relationship between BCP architecture, membrane structure, and performance, the permeation of the model dye methyl orange was evaluated for a series of ISV membranes with varying molar mass. As previously reported by Dorin et al. [25], membranes fabricated from ISV terpolymers with similar volume fractions but increasing molar mass are characterized by increasing pore diameters. As a result, ISV membrane water and polymer solute rejection performance could be systematically tuned through tailoring of terpolymer molar mass. The present

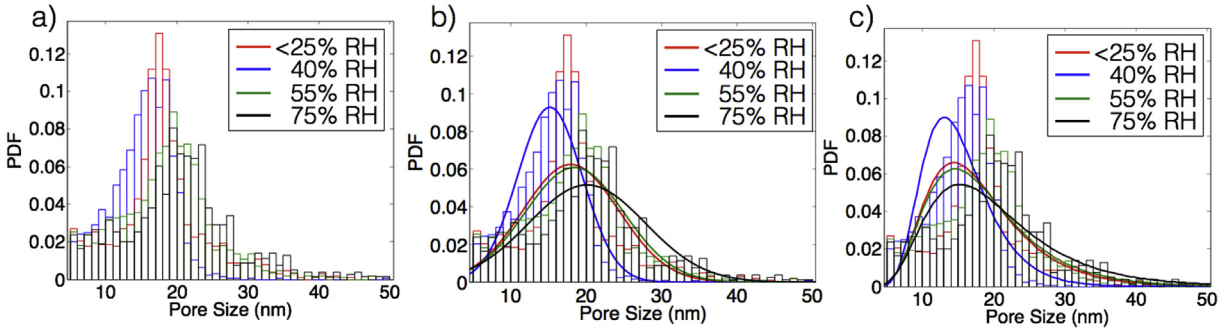

Fig. 4. Pore size distribution analyses of ISV119 membranes cast at varying RH from polymer casting solutions of 11 wt%. a) pore size histograms; b) histograms with corresponding normal Gaussian fits ($\sigma/\mu = 0.36$, 0.28, 0.36, and 0.38 for 25%, 40%, 55%, and 75% RH, respectively); c) histograms with corresponding log-normal fits ($\sigma/\mu = 0.14$, 0.12, 0.14, and 0.15 for 25%, 40%, 55%, and 75% RH, respectively).

Table 3
Diffusion coefficient of methyl orange diffusing through ISV119 membranes cast from 40% to 75%RH together with membrane pore size analysis results.

Polymer	D(exp) (x10^{-8} cm^2/s)[a]	ε	$r_p = \mu$	σ
ISV119 40% RH	3.3 t_{lag} = 8.3 min	15.76%	7.9	2.5
ISV119 75% RH	0.8 t_{lag} = 33 min	18.34%	10.7	4.7

Average pore size (r_p or μ) and porosity (ε) determined from ImageJ analysis and σ calculated from log normal fits (see text).
[a] As determined through the time-lag method (Eqn. (3)).

study was designed to assess small molar mass solute transport through ISV membranes as a function of molar mass.

Membranes fabricated from varying molar mass terpolymers were prepared by dissolving the triblock terpolymer into a binary solvent system of 7/3 DOX/THF by weight ratio. Supported membranes were cast from a 16 wt% ISV43, 12 wt% ISV99, and 11 wt% ISV119 polymer solution pipetted directly onto a 0.1 μm nylon support (Sterlitech Inc.) with an evaporation time of 100 s and the optimized casting condition of 40% RH. SEM micrographs of the top surfaces are shown in Fig. 6. All membrane top surfaces are characterized by highly ordered pores forming square lattices.

The ISV43, ISV99, and ISV119 membranes were subjected to pH 7 ("open" state) and pH 4 ("closed" state) solutions of methyl orange as described above. The 0.1 M buffer solutions used in the permeation experiments is expected to screen the electrostatics associated with the charged dye molecule. The cumulative amount of diffusant through the membranes in different states over time is shown in Fig. 7 with corresponding calculated values of D(exp) listed in Table 4.

Under neutral conditions ("open" state), the permeation rate of methyl orange increased with ISV terpolymer molar mass. While this is the expected behavior, closer inspection reveals that this trend is based on two different effects. Average pore size from image analysis (see Table 4) first increases from 10 nm for ISV43 to 18 nm for ISV99, but then decreases to 16 nm for ISV119. Therefore, pore size alone cannot explain the observed trend in P(exp) in Table 4.

Interestingly, for the molar mass series of terpolymer membranes studied here contrary to expected behavior the pore density increases with molar mass (Table 4, right side). So while moving from ISV99 to ISV119 average pore size decreases from 18 to 16 nm, pore density increases from 7.2 to 8.0 × 10^{14} pores/m^2. Together

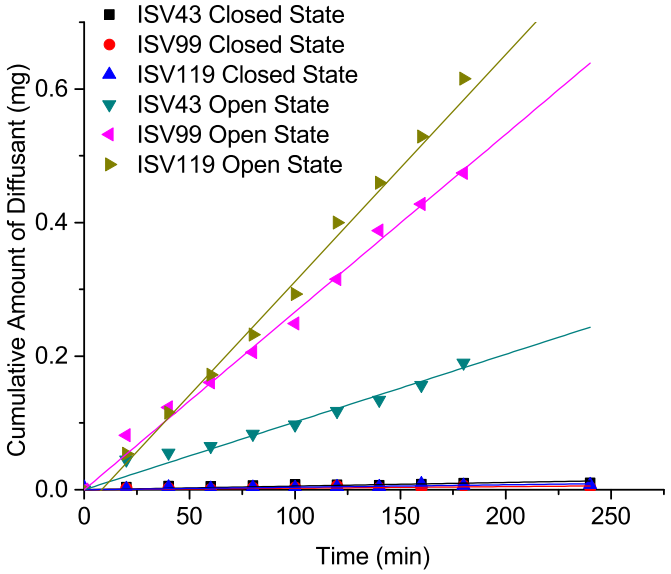

Fig. 7. Cumulative amounts of methyl orange permeated through varying molar mass ISV triblock terpolymer membranes for open and closed states.

with differences in substructure not assessed here, this may account for the increased diffusion of the small molar mass model solute. The low pore density of ISV43 membranes may be due to closed pores, unrecognized by ImageJ during analysis, compare top surface SEM images in Fig. 6.

As expected, under acidic conditions ("closed" state), the permeation rate again is reduced to a minimal amount for all membranes tested (compare Figs. 5 and 7). In the "closed" state, pores are effectively closed preventing diffusion of methyl orange through the membranes. The lack of diffusion through the ISV membrane is likely a result of pore size changes and not primarily an effect of electrostatics. This is supported by the fact that the charge of the methyl orange dye in the 0.1 M buffer solution is expected to be fully screened. The change in permeation rate from 220 × 10^{-8} cm^2/s ("open" state) to 2.5 × 10^{-8} cm^2/s ("closed" state) for ISV119 membranes can be regarded as an "on" and "off" switch brought on by pH changes.

In order to provide deeper insights into the effects of membrane structure on small molar mass solute transport, experimental results were compared to theoretical predictions. It is essential to

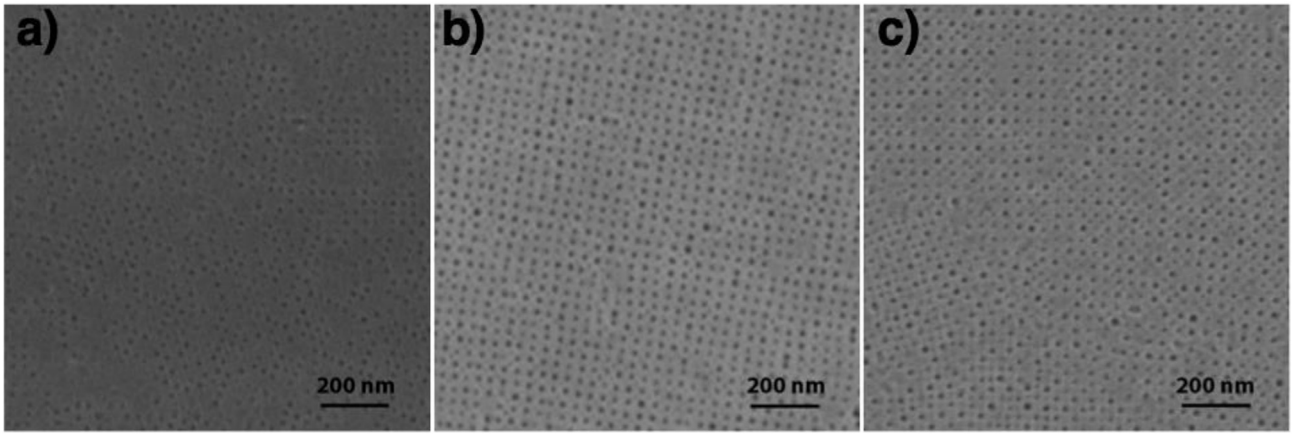

Fig. 6. SEM characterization of top surfaces of ISV membranes from a) ISV43, b) ISV99, and c) ISV119, all cast at 40% RH. Supported membranes were cast from a 16 wt% ISV43, 12 wt % ISV99, and 11 wt% ISV119 polymer solution in 7/3 DOX/THF pipetted directly onto a 0.1 μm nylon support (Sterlitech Inc.) with an evaporation time of 100 s.

Table 4
Diffusion and permeability coefficients of methyl orange permeating through different ISV membranes for closed and open states together with membrane pore size analysis results.

Polymer	Closed State	Open State	Open State	Pore density	ε	$r_p = \mu$	σ
	D(exp)[b] (x10^{-8} cm^2/s)	D(exp) (x10^{-8} cm^2/s)	P(exp)[a] (x10^{-5} cm/s)	(x10^{14} pores/m^2)			
ISV43	15.3	280[b]	1.1	4.6	3.86%	5.2	1.4
ISV99	1.4	160[b]	2.9	7.2	18.33%	9.0	2.0
ISV119	2.5	220[b]/3.3[c] t_{lag} = 8.3 min	3.5	8.0	15.76%	7.9	2.5

Average pore size (r_p or μ) and porosity (ε) determined from ImageJ analysis and σ calculated from log normal fits (see text).
[a] As determined from Eqn. (4) *i.e.*, P(exp) = slope/(AC).
[b] As determined through Eqn. (4).
[c] As determined through the time-lag method (Eqn. (3)).

characterize the entirety of the cross section of ISV membranes for permeation analysis. ISV membranes are characterized by a surface separation layer, which has a simple cubic structure [3,17] (~100–200 nm thick; described above) on top of a 3D interconnected macroporous sponge-like substructure. Furthermore, the relatively thick (~50–60 μm) and asymmetric sponge type substructure of these ISV membranes consists of macropore walls that themselves are mesoporous (i.e. the substructure is not only asymmetric, but truly hierarchical) [3]. This is in stark contrast to what has been described for PS-*b*-P4VP diblock copolymer derived UF membranes [2]. Therefore, we expect tortuous paths for solute molecules through these mesopores all the way through the entire membrane. As a result, in order to simplify the theoretical description, we used the hindered diffusion model and assumed a constant porosity throughout. For example, the measured diffusion coefficient, D(exp), of methyl orange dye in UF membrane ISV99 in the open state at pH 7 (160×10^{-8} cm^2/s) is about a factor of three lower than the bulk solution value that is calculated using the Stokes-Einstein relationship, $D_w = k_bT/(6\pi\,\eta\,r_s) \sim 5.4 \times 10^{-6}$ cm^2/s (where k_b is Boltzmann's constant, T = 25 °C, η is the viscosity of water at 25 °C, and the solute radius is estimated from Eqn. (6) as r_s = 0.45 nm). Based on the hydrodynamic theory for hindered diffusion of a solid, spherical solute through an array of cylindrical pores with comparable size as described by the Renkin equation (Eqn. (5)), theoretical diffusion coefficients, $D(\lambda)$, were calculated for the different ISV terpolymer membranes as listed in Table 5. A hindered diffusion model was chosen to simplify solute diffusion through the complex pore structures of ISV membranes using the whole membrane thickness of l = 100 μm. Here we note that the assumption of continuity of the cylindrical nanopore structure of the separation layer across the total membrane thickness is not consistent with the actual membrane structure that shows a graded morphology with interconnected meso- and macroporous regions (*vide infra*). Nevertheless, in the absence of a complete description of the membrane structure, the applied approximation was found to be helpful to interpret transport in terpolymer based UF membranes. Following this approach, the diffusion coefficients (for ISV119 membranes) were determined through Eqn. (3) (time-lag method) and Eqn. (4), for comparison. Additionally, theoretical permeability coefficients, $P(\lambda)$, were determined as a function of solute-to-pore size ratio and tortuosity (Eqn. (7)). In order to compare experimental and theoretical permeability coefficients, $P(\lambda)$ values were first calculated assuming a membrane thickness of l = 100 μm and without taking tortuosity into account (i.e. τ = 1). The resulting values were within the same order of magnitude as P(exp) (compare columns 2 and 4 in Table 5).

As evidenced in earlier studies by cross sectional SEM images, neither separation layer nor substructure of ISV terpolymer membranes consist of vertical cylindrical pores. For example, in the separation layer the cubic pore network is characterized by vertical and horizontal channels [3,6–8,11]. The solutes' pathway is therefore expected to be very tortuous as molecules can move vertically as well as horizontally through the selective layer. By equating P(exp) to $P(\lambda)$, calculated values of τ, used here as a fitting parameter, fall close to the typical tortuosity range of 1.5–2.5 [27] for mesoporous membranes. These results suggest that the combined effects of hydrodynamic hindered diffusion and pore tortuosity can account for the observed small molar mass solute transport through ISV based UF membranes taking into account the entire membrane thickness (l = 100 μm).

For comparison $P(\lambda)$ values were also calculated assuming that only the selective top separation layer with l = 100 nm contributes to hindered diffusion. It is obvious from Table 5 that this does not provide satisfactory results as theoretical $P(\lambda, \tau = 1)$ values now are different by orders of magnitude from the experiments (compare $P(\lambda)$ in column 6 with P(exp) in column 2). Furthermore, matching experimental with theoretical results would require non-physical tortuosity values as also shown in Table 5 (column 7).

4. Conclusion

In summary, ISV membranes derived from the SNIPS process

Table 5
Summary of diffusion and permeability coefficients from theoretical predictions and experimental data.

Membrane	P(exp)[a] (x10^{-5} cm/s)	$D(\lambda)$ (x10^{-6} cm^2/s)	$P(\lambda)$ (x10^{-5} cm/s) τ = 1 l = 100 μm	τ[d] l = 100 μm	$P(\lambda)$ (x10^{-2} cm/s) τ = 1 l = 100 nm	τ[d] l = 100 nm	D(exp) (x10^{-6} cm^2/s) τ = 1
ISV43	1.1	3.7	1.4	1.3	1.4	1300	2.8[b]
ISV99	2.9	4.4	8.0	2.8	8.0	2800	1.6[b]
ISV119 (40% RH)	3.5	4.2	6.6	1.9	6.6	1900	2.2[b] (0.033[c]; t_{lag} = 8.3 min)
ISV119 (75% RH)	1.5	4.5	8.3	5.5	8.3	5500	0.8[b] (0.008[c]; t_{lag} = 33 min)

[a] As determined from Eqn. (4) *i.e.*, P(exp) = slope/(AC).
[b] As determined from Eqn. (4), D(exp) = P(exp) (τl)/ε (assuming τ = 1).
[c] As determined by the time-lag method (Eqn. (3)).
[d] As determined by equating P(exp) to $P(\lambda, \tau)$.

were fabricated from ISV triblock terpolymers ranging in molar mass from 43 kg/mol to 119 kg/mol at varying levels of RH during the casting process. Investigations into the influence of RH on membrane surface structure revealed that ISV membranes exhibited optimal surface ordering and pore density when cast at mid range values around 40–45% RH. The observed structural changes correlated with differences in permeation rate of a model small molar mass solute through membranes cast at optimal and non-optimal RH, with higher diffusivity observed in the membrane characterized by a more ordered surface structure obtained at optimal RH.

Analysis into the relationship between triblock terpolymer molecular size and diffusion performance revealed that membranes fabricated from higher molar mass ISV terpolymers exhibited higher small molar mass solute diffusivity. Results could be rationalized by taking into account observed membrane pore size and pore density. Moreover, combining predictions of a hydrodynamic theory assuming hindered diffusion of a solid, spherical solute through an array of cylindrical pores of comparable size with the effect of pore tortuosity, observed values of the small molar mass solute permeability coefficients could only be accounted for when the entire membrane thickness ($l = 100$ μm) rather than only the thickness of the top separation layer ($l = 100$ nm) was used in the calculations.

The ability to extend the use of SNIPS membranes away from regular separation applications and towards the use as well-controlled delivery vehicles rests on tuning membrane properties via BCP molecular design and architecture as well as on finding optimal membrane casting conditions. This study suggests that through tailoring of BCP molar mass and relative humidity during casting, the rate of release and diffusion of solutes through SNIPS membranes can be controlled for targeted performance.

Acknowledgments

The authors would like to acknowledge funding of this work by the FLIR Systems, Inc. and the Defense Threat Reduction Agency (DTRA) Contract No. HDTRA1-13-C0003. This work utilized the Cornell Center for Materials Research (CCMR) facilities supported by NSF MRSEC program (DMR-1120296). Y.G. acknowledges funding by the National Science Foundation (DMR-1409105).

References

[1] R.M. Dorin, D. Salomon Marques, H. Sai, U. Vainio, W.A. Phillip, K.V. Peinemann, S.P. Nunes, U. Wiesner, Solution small angle X ray scattering as a screening and predictive tool in the fabrication of asymmetric block copolymer membranes, ACS Macro Lett. 1 (2012) 614–617.
[2] K.V. Peinemann, V. Abetz, P.F.W. Simon, Asymmetric superstructure formed in a block copolymer via phase separation, Nat. Mater 6 (2007) 992–996.
[3] W.A. Phillip, R.M. Dorin, J. Werner, E.M. Hoek, U. Wiesner, M. Elimelech, Tuning structure and properties of graded triblock terpolymer-based mesoporous and hybrid films, Nano Lett. 11 (2011) 2892–2900.
[4] R.A. Mulvenna, J.L. Weidman, B. Jing, J.A. Pople, Y. Zhu, B.W. Boudouris, W.A. Phillip, Tunable nanoporous membranes with chemically-tailored pore walls from triblock polymer templates, J. Membr. Sci. 470 (2014) 246–256.
[5] Q. Zhang, Y. Gu, Y.M. Li, P.A. Beaucage, T. Kao, U. Wiesner, Dynamically responsive multifunctional asymmetric triblock terpolymer membranes with intrinsic binding sites for covalent molecule attachment, Chem. Mater 28 (2016) 3870–3876.
[6] Y.M. Li, D. Srinivasan, P. Vaidya, Y. Gu, U. Wiesner, Asymmetric membranes from two chemically distinct triblock terpolymers blended during standard membrane fabrication, Macromol. Rapid Commun. 37 (2016) 1689–1693.
[7] Q. Zhang, Y.M. Li, Y. Gu, R.M. Dorin, U. Wiesner, Tuning substructure and properties of supported asymmetric triblock terpolymer membranes, Polymer 107 (2016) 398–405.
[8] M.M. Pendergast, R.M. Dorin, W.A. Phillip, U. Wiesner, E.M.V. Hoek, Understanding the structure and performance of self-assembled triblock terpolymer membranes, J. Membr. Sci. 444 (2013) 461–468.
[9] S. Rangou, K. Buhr, V. Filiz, J.I. Clodt, B. Lademann, J. Hahn, A. Jung, V. Abetz, Self-organized isoporous membranes with tailored pore sizes, J. Membr. Sci. 451 (2014) 266–275.
[10] A. Jung, S. Rangou, C. Abetz, V. Filiz, V. Abetz, Structure formation of integral asymmetric composite membranes of polystyrene-block-poly (2-vinylpyridine) on a nonwoven, Macromol. Mater. Eng. 297 (2012) 790–798.
[11] Y. Gu, U. Wiesner, Tailoring pore size of graded mesoporous block copolymer membranes: moving from ultrafiltration toward nanofiltration, Macromol 48 (2015) 6153–6159.
[12] S.P. Nunes, R. Sougrat, B. Hooghan, D.H. Anjum, A.R. Behzad, L. Zhao, N. Pradeep, I. Pinnau, U. Vainio, K.V. Peinemann, Ultraporous films with uniform nanochannels by block copolymer micelles assembly, Macromol 43 (2010) 8079–8085.
[13] V. Abetz, Isoporous block copolymer membranes, Macromol. Rapid Commun. 36 (2015) 10–22.
[14] C. Stegelmeier, V. Filiz, V. Abetz, J. Perlich, A. Fery, P. Ruckdeschel, S. Rosenfeldt, S. Förster, Topological paths and transient morphologies during formation of mesoporous block copolymer membranes, Macromol 47 (2014) 5566–5577.
[15] L. Oss-Ronen, J. Schmidt, V. Abetz, A. Radulescu, Y. Cohen, Y. Talmon, Characterization of block copolymer self-assembly: from solution to nanoporous membranes, Macromol 45 (2012) 9631–9642.
[16] D.S. Marques, R.M. Dorin, U. Wiesner, D.M. Smilgies, A.R. Behzad, U. Vainio, K.V. Peinemann, S.P. Nunes, Time-resolved GISAXS and cryo-microscopy characterization of block copolymer membrane formation, Polymer 55 (2014) 1327–1332.
[17] Y. Gu, R.M. Dorin, K.W. Tan, D.M. Smilgies, U. Wiesner, In situ study of evaporation-induced surface structure evolution in asymmetric triblock terpolymer membranes, Macromol 46 (2016) 4195–4201.
[18] B. Sutisna, G. Polymeropoulos, V. Musteata, K.V. Peinemann, A. Avgeropoulos, D.M. Smilgies, N. Hadjichristidis, S.P. Nunes, Design of block copolymer membranes using segregation strength trend lines, Mol. Syst. Des. Eng. 1 (2016) 278–289.
[19] S.Y. Yang, J.A. Yang, E.S. Kim, G. Jeon, E.J. Oh, K.Y. Choi, S.K. Hahn, J.K. Kim, Single-file diffusion of protein drugs through cylindrical nanochannels, ACS Nano 4 (2010) 3817–3822.
[20] J. Crank, The Mathematics of Diffusion, Oxford University Press, Oxford, 1975.
[21] R.A. Siegel, E.L. Cussler, Reactive barrier membranes: some theoretical observations regarding the time lag and breakthrough curves, J. Membr. Sci. 229 (2004) 33–41.
[22] E.M. Renkin, Filtration, diffusion, and molecular sieving through porous cellulose membranes, J. Gen. Physiol. 38 (1954) 225–243.
[23] W.R. Bowen, A.W. Mohammad, Characterization and prediction of nanofiltration membrane performance—a general assessment, Chem. Eng. Res. Des. 76 (1998) 885–893.
[24] M. Mitsuishi, A. Datyner, Diffusion of methyl orange and its homologs in water and in micellar solution of dodecyltrimethylammonium bromide, Sen'i Gakkaishi 36 (1980) T175–T178.
[25] R.M. Dorin, W.A. Phillip, H. Sai, J. Werner, M. Elimelech, U. Wiesner, Designing block copolymer architectures for targeted membrane performance, Polymer 55 (2014) 347–353.
[26] K.H. Youm, S.W. Kim, Prediction of intrinsic pore properties of ultrafiltration membrane by solute rejection curves: effects of operating conditions on pore properties, J. Chem. Eng. Jpn. 24 (1991) 1–7.
[27] R.W. Baker, Membrane Technology and Applications, England, 2004.